The Spectral Emission Characteristics of Laser Induced Plasma on Tea Samples*

ZHENG Peichao (郑培超)[1,2], SHI Minjie (石珉杰)[1], WANG Jinmei (王金梅)[1], LIU Hongdi (刘红弟)[1]

[1]Chongqing Municipal Level Key Laboratory of Photo-Electronic Information Sensing and Transmitting Technology, College of Optoelectronic Engineering, Chongqing University of Posts and Telecommunications, Chongqing 400065, China

[2]State Key Laboratory of Power Transmission Equipment & System Security and New Technology, Chongqing University, Chongqing 400065, China

Abstract Laser induced breakdown spectroscopy (LIBS) provides a useful technique for food security as well as determining nutrition contents. In this paper, optical emission studies of laser induced plasma on commercial tea samples were carried out. The spectral intensities of Mg, Mn, Ca, Al, C and CN vibration bands varying with laser energy and the detection delay time of an intensified charge coupled device were studied. In addition, the relative concentrations of six microelements, i.e., Mg, Mn, Ca, Al, Na and K, were analyzed semi-quantitatively as well as H, for four kinds of tea samples. Moreover, the plasma parameters were explored, including electron temperature and electron number density. The electron temperature and electron number density were around 11000 K and 10^{17} cm^{-3}, respectively. The results show that it is reasonable to consider the LIBS technique as a new method for analyzing the compositions of tea leaf samples.

Keywords: LIBS, tea leaves, relative concentration, plasma parameters

PACS: *52.50.Jm, 52.38.Mf*

DOI: 10.1088/1009-0630/17/8/09

(Some figures may appear in colour only in the online journal)

1 Introduction

In the past few decades, many detection methods, such as microwave plasma torch-atomic emission spectroscopy (MPT-AES), flame atomic absorption spectroscopy (FAAS), etc., have been proposed for the determination of microelements in organic plant samples, including tea leaves, *Cardiocrinum giganteum* and pagoda flowers, etc [1−3]. Techniques such as MPT-AES and FAAS have good detection limits and measurement accuracy for these plant samples, but they require complicated sample preparation and prove difficult in achieving rapid, non-destructive and real-time detection. Laser-induced breakdown spectroscopy (LIBS) is a type of atomic emission spectroscopy where the output from a pulsed laser is focused onto a sample to create an intense plasma. The sample is heated by the laser pulse and more electrons are created through ionization. Cascade ionization takes place during the pulse duration and a plasma plume is produced in front of the sample [4]. The advantages of LIBS over other conventional spectrometric analytical methods include rapid analysis, minimal sample preparation, its practically nondestructive nature, operational simplicity, real-time analysis and the versatile sampling of solids [5−9], liquids [10−14], gases [15−17] and aerosols [18−20]. Moreover, LIBS is able to perform elemental determinations *in situ* using portable instruments and to investigate samples remotely using stand-off analysis [21].

Statistical methodologies such as linear correlation, principal components analysis and the soft independent model of class analogy have already been used in many fields of spectral data analysis [22]. Munson [23], Morel [24] and Baudelet [25] applied the LIBS technique to the experiments of distinguishing bacteria and microbes respectively, and they also compared and analyzed the result of data processing, and got good results. Aragon et al. [26]analyzed the relative standard deviations (RSDs) in steel using the LIBS technique and obtained higher precision. These works increased the accuracy of LIBS in applications to food safety monitoring, bacterium identification and microelement analysis.

In this paper, the spectra of four kinds of tablets of pressed tea leaf samples were analyzed. Variations

of the spectral line intensities, such as some microelements, organic elements and molecular bands, were studied as functions of the laser energy and the ICCD detection delay time. The RSDs and relative concentrations of six microelements (Mg, Mn, Ca, Al, Na and K) and organic element H were compared and analyzed. The plasma parameters (electron temperature T_e and electron number density N_e) of the four kinds of tea leaf samples were also compared.

2 Experimental details

2.1 Experimental set-up

A schematic view of the experimental set-up is presented in Fig. 1. A Q-switched Nd:YAG laser (Big Sky Laser Technology, Ultra 100), at a fundamental wavelength of 1064 nm with a pulse duration of 8 ns, a repetition rate of 20 Hz and a maximum pulse energy of 100 mJ, was used as the excitation laser. The energy of the laser could be adjusted by changing the Q delay time, which could be evaluated using an optical power meter. The laser beam was focused perpendicular to the surface of the sample on a two-dimensional translation stage, which was controlled by a controller (Zolix SC300-2A) with a planoconvex lens ($f = 100$ mm) to produce an intense, transient plasma. The light emitted from the plasma was focused by a microscope objective lens system and collected by a 2 m long multimode silica fiber. The light was then transmitted through the fiber to the entrance of a computerized Czerny–Turner spectrograph (Andor Model SR-750 A). The spectrograph was equipped with three ruled gratings, 2400 grooves/mm, 1200 grooves/mm and 300 grooves/mm, which were interchangeable under computer control, providing high and low resolution spectra in the wavelength range of 200-900 nm. A gated and intensified CCD (ICCD) camera (Andor DH340T-18U-03) was coupled to the output end of the spectrograph. The ICCD camera had 2048×512 pixels and was cooled to –15 °C by a Peltier cooler to reduce noise. Twenty laser pulses were accumulated to obtain each spectrum and each experimental condition analyzed using LIBS is the average of ten spectrum measurements to increase the sensitivity and reduce the standard deviation.

2.2 Sample preparation

Four commercial tea leaf samples were analyzed in this work, i.e., black tea (Anxi, Fujian), Huangya tea (Ya'an, Sichuan), Longjing tea and Pu'er tea (Pu'er, Yunnan). Because tea leaves are irregular and granular solid samples, the samples had to be preprocessed by tablet pressing in order to reduce the experimental errors and obtain a better ablation efficiency and higher repeatability in the LIBS measurements. Before tablet pressing, all the tea leaf samples were dried in a drying oven at 70 °C for 5 h. Then each tea sample was ground

into powders for 2 h. These tea powders were pressed into tablets (13 mm in diameter and 2 mm thick) using a hydraulic press (4 min under 30 MPa for each tablet).
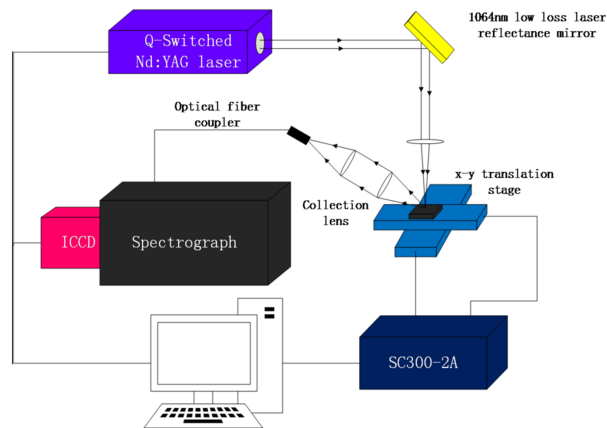

Fig.1 Schematic diagram of the LIBS experimental set-up

3 Results and discussion

3.1 Spectral line analysis

Fig. 2 shows the LIBS spectrum of the Longjing tea leaves from 200 nm to 800 nm. The spectral lines of metallic elements such as Ca, Na, Al, K, Fe, Mg and Mn, the organic elements C, H, O and N, and the vibrational band of CN are found in Fig. 2 according to the NIST database [27] and Refs. [24,28-30]. Some of the spectral lines of O and N are certainly caused by O_2 and N_2 in the air and the others are caused by O and N in the tea sample. Some of the molecular spectral lines of CN are caused by CN diatomic molecules in the Longjing tea leaves, the others are caused by the combination reaction ($C_2 + N_2 \rightarrow 2CN$) of elemental C in the Longjing tea leaves and N in the air. These two kinds of CN molecular spectral lines can be distinguished by the TRLIBS technique due to their different decay times [24].
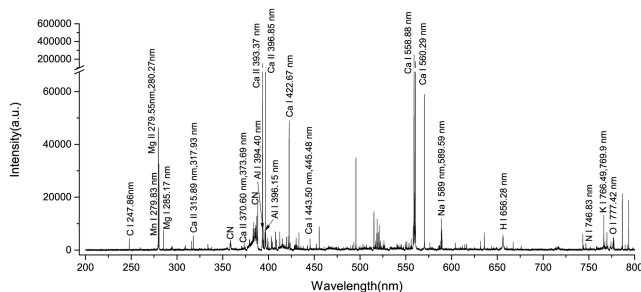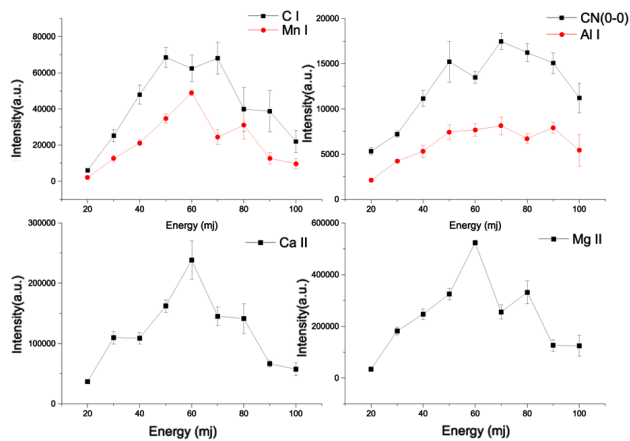

Fig.2 LIBS spectrum of the Longjing tea leaf sample at a 2 μs ICCD detection delay, 2 μs gate width and 50 mJ laser pulse energy

3.2 Effects of laser energy and detection delay time

The variations of the spectral lines of C(I)(247.86 nm), Mg(II)(279.55 nm), Mn(I)(279.83 nm),

Ca(II)(393.37 nm), Al(I)(396.15 nm) and CN(0-0)(388.34 nm) in the Longjing tea leaf sample were studied in relation to the laser energy and the ICCD detection delay time. Fig. 3 presents the intensity evolution of these spectral lines as the laser energy is varied from 20 mJ to 100 mJ (the sampling interval is 10 mJ), when the ICCD delay time is 2 μs and the gate width is 2 μs.
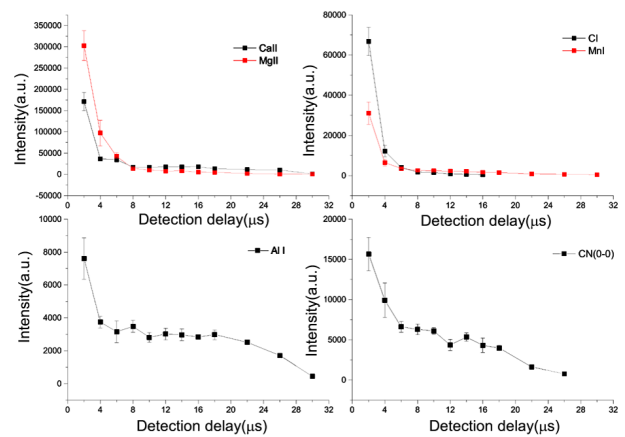

Fig.3 Intensity variations of the C(I)(247.86 nm), Mg(II)(279.55 nm), Mn(I)(279.83 nm), Ca(II)(393.37 nm), Al(I)(396.15 nm) and CN(0-0)(388.34 nm) spectral lines of the Longjing tea leaf sample with laser energy

At the beginning, the characteristic spectral lines have high intensities as well as background noise and then the intensities of both the characteristic spectral lines and background noise decrease. But the background noise decreases much faster than the intensities of the characteristic spectral lines and the characteristic spectral lines can be distinguished more obviously from the background noise. After 32 μs, there are no longer any characteristic spectral lines.

The curves first rise and then fall for the spectral lines of all six elements. It is observed that the intensities of the spectral lines increase monotonically with laser energy while the energy is lower than 50 mJ. Once the laser energy is higher than 50 mJ, the intensities of the spectral lines no longer increase with laser energy, and even decrease when the laser energy exceeds 60 mJ. Overall, the standard deviations increase with laser energy. Higher laser energy produces greater ablation and higher intensities of the spectral lines are obtained at higher laser energies. But excessively high laser energy will destroy the tablet pressed samples and create a much larger ablation crater. In addition, a larger amount of powder is produced above the sample, which decreases the intensities and stabilities of the spectral lines and causes higher standard deviations.

Fig. 4 shows the variations in the intensities of the C(I)(247.86 nm), Mg(II)(279.55 nm), Mn(I)(279.83 nm), Ca(II)(393.37 nm), Al(I)(396.15 nm) and CN(0-0)(388.34 nm) spectral lines from the Longjing sample when the ICCD detection delay time is varied from 2 μs to 30 μs (the sampling interval is 2 μs) at a 2 μs gate width and 50 mJ laser pulse energy. The maximum in-

tensities are observed at 2 μs after which the intensities decrease rapidly with ICCD detection delay time. The intensities of the ionic spectral lines (Ca(II)(393.37 nm) and Mg(II)(279.55 nm)) decrease much faster than the atomic lines (C(I)(247.86 nm), Mn(I)(279.83 nm) and Al(I)(396.15 nm)) and molecular line (CN(0-0)(388.34 nm)) at the beginning. The lifetime of the spectral line of the organic element C(I)(247.86 nm) is the shortest and cannot be distinguished from the background noise after 16 μs. The spectral intensity of the CN(0-0)(388.34 nm) molecular line decreases the most slowly.

Fig.4 Intensities of the C(I)(247.86 nm), Mg(II)(279.55 nm), Mn(I)(279.83 nm), Ca(II)(393.37 nm), Al(I)(396.15 nm) and CN(0-0)(388.34 nm) spectral lines from the Longjing tea leaves versus the ICCD delay times

3.3 Semi-quantitative analysis

Four kinds of tea leaves were selected to perform qualitative and semi-quantitative analyses, while the parameters of the LIBS were 50 mJ laser pulse energy, 2 μs ICCD detection delay time and 10 μs gate width. As shown in Fig. 5, the characteristic spectral lines of C, Mn, Mg, Ca, CN, Al, Fe, Na, H, N, O and K were found in all four samples.

Seven spectral lines, Mg(II)(279.55 nm), Mn(I)(279.83 nm), Ca(II)(393.37 nm), Al(I)(396.15 nm), Na(I)(589.59 nm), H(I)(656.28 nm) and K(I)(766.49 nm), were chosen for analysis for the four kinds of samples. In order to avoid the interference of other emissions and the self-absorption effect in the analyses of the spectral lines [31], the spectral line of the dominant element C(I)(247.86 nm) was chosen as the reference spectral line. The relative concentrations of Mg, Mn, Ca, Al, Na, H and K among the four tea leaf samples were determined and analyzed.

Table 1 shows the RSDs for relative concentrations of Mg, Mn, Ca, Al, Na, H and K. The RSDs of these four sample are less than 25%. The RSDs of the Huangya tea leaves are obviously higher than the others in Table 1, because Huangya tea leaves are needle-shaped and more difficult to grind than the other samples. Therefore Huangya tea leaves are less homogeneous under the same sample processing conditions. The RSDs of Ca and H in the Pu'er tea leaves are the highest for
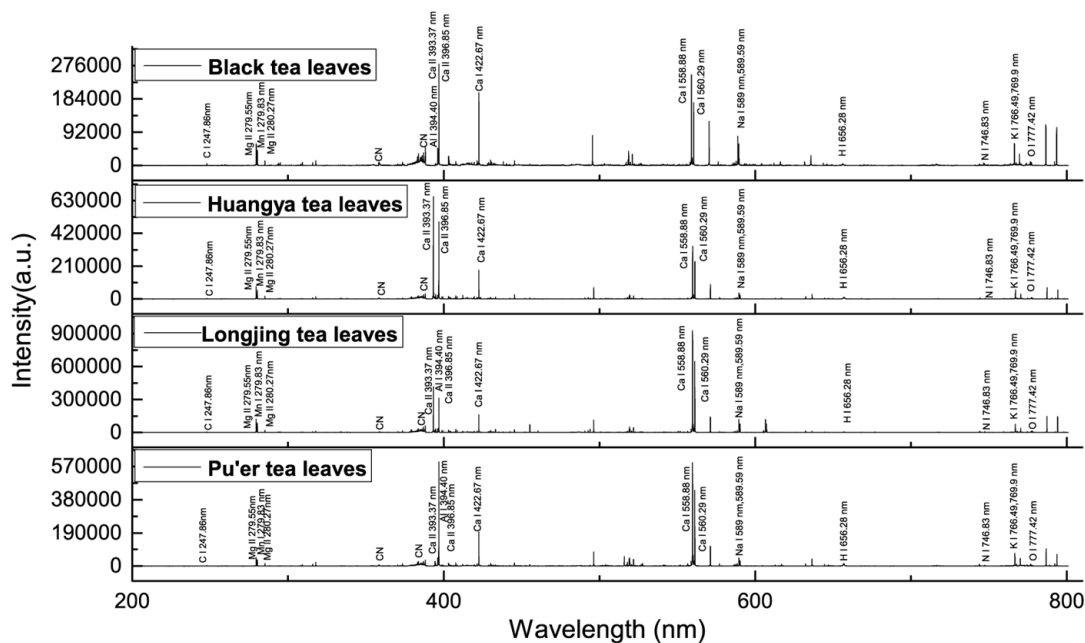
Fig.5 Qualitative comparison among the four kinds of tea leaf samples from 200 nm to 800 nm

Table 1. RSDs of the relative concentrations of Mg, Mn, Ca, Al, Na, H and K

Tea leaves	Mg/C	Mn/C	Ca/C	Al/C	Na/C	H/C	K/C
Black tea leaves (%)	5.43	7.02	4.64	8.89	13.15	13.58	2.93
Huangya tea leaves (%)	15.70	15.57	18.32	31.63	18.80	15.28	7.14
Longjing tea leaves (%)	8.83	10.48	8.08	10.74	9.79	9.82	5.93
Pu'er tea leaves (%)	9.05	9.85	24.59	11.67	11.06	22.69	6.70

the four kinds of samples, because the Pu'er tea leaf samples are the loosest sample of the four kinds of tea leaves.

Fig. 6 shows the semi-quantitative analytical results for the four tea leaf samples. The black tea leaves and Longjing have similar relative concentration values for Mg of 3.64 and 3.74, respectively, while Pu'er has the highest concentration value of 6.01 and Huangya has the lowest of 3.14. The relative concentration values of Mn are 0.35 for black tea leaves and 0.39 for Longjing with the highest value being 0.55 for Pu'er and the lowest 0.31 for Huangya. For the relative concentration values of Ca, the black tea leaves and Longjing have higher values of 3.97 and 4.08, respectively, with 2.76 for Huangya and 3.37 for Pu'er. For Al, Pu'er tea leaves have a much higher relative concentration value of 0.47, while the values are 0.25, 0.13 and 0.19 for black, Huangya and Longjing tea leaves, respectively. The highest relative concentration value of Na is 0.61 for Longjing with 0.38 for black, 0.37 for Huangya and 0.29 for Pu'er, respectively. For H, black tea leaves have the highest relative concentration value of 0.09, Pu'er has a middle value of 0.05, while the values are 0.03 and 0.04 for Huangya and Longjing, respectively, which shows that there is still a lot of moisture content involved in the four kinds of tea leaf samples. The relative concentration values of K are 0.42, 0.43 and 0.41 for black tea leaves, Huangya and Longjing, re-
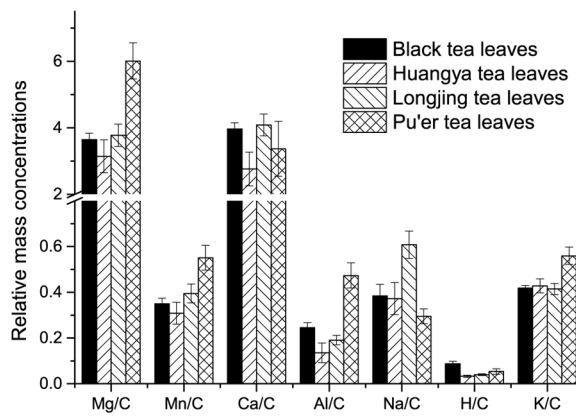
spectively, with a higher value of 0.56 for Pu'er.

Fig.6 Semi-quantitative analytical results for the four tea leaves samples. The error bars in each panel represent the standard deviations

The black, Huangya, Longjing and Pu'er tea leaves are 80% fermented tea, 10%-20% fermented tea, 0% fermented tea and 100% fermented tea, respectively. Huangya and Longjing are unfermented teas while the black and Pu'er teas are completely fermented tea. There are obvious differences in the relative concentrations of the seven elements in the four tea leaf samples. Pu'er tea leaves have the highest relative concentrations of Mg, Mn, Al and K. The relative concentrations of Al

in the Pu'er tea leaves and black tea leaves (completely fermented tea) are higher than those in Longjing and Huangya (unfermented tea). The difference in the relative concentrations of elements in tea samples can be ascribed to many causes such as the different species of tea, the degree of fermentation, the degree of maturity of the tea leaves, the local water and soil, or some other parameters.

4 Plasma parameters

4.1 Electron temperature and electron number density

The determination of plasma parameters, including electron temperature T_e and electron number density N_e, is essential for understanding the mechanisms of the LIBS technique. The electron temperature was determined using the Boltzmann plot method from the intensities of the observed lines, which are normally proportional to the population of the pertinent upper level. The following relation was used to extract the electron temperature [32]:

$$\ln\left(\frac{I_{ki}\lambda_{ki}}{A_{ki}g_k}\right) = -\frac{E_k}{k_B T_e} + \ln\left(\frac{N(T)}{U(T)}\right), \qquad (1)$$

where k_B is the Boltzmann constant, $U(T)$ is the partition function, I_{ki} is the integrated line intensity of the transition involving an upper level (k) and lower level (i), λ_{ki} is the transition wavelength, A_{ki} is the transition probability, g_k is the statistical weight of level (k), $N(T)$ is total particle number density, E_k is the energy of the upper level and T_e is the electron temperature. Eq. (1) leads to a liner plot of $\ln(\lambda I/Ag)$ versus the energy term E_k, and the electron temperature can be deduced from the slope of the fitting straight line. Thus the electron temperature can be determined without knowing the total particle number density or the partition function.

In these experiments, the spectral lines of Ca(II)(317.93 nm), Ca(II)(370.60 nm), Ca(II)(373.69 nm), Ca(II)(393.37 nm) and Ca(II)(396.85 nm) were selected to calculate the electron temperature. The spectroscopic data, such as wavelength (λ), statistical weight (g), transition probability (A) and energy (E), listed in Table 2 can be found in the NIST database [27].

During the evolution of a laser induced plasma, excitation and ionization take place in the evaporated ma-

terial. The electron number density is a crucial parameter for determining the elemental composition. In fact, there are two main line broadening mechanisms in laser induced plasmas, i.e., Stark broadening and Doppler broadening. At higher electron number densities, Stark broadening induced by collisions with charged particles dominates. The electron number density can be determined from the Stark broadened line profile of an isolated line of either a neutral atom or a single charged ion. The full width at half maximum (FWHM) $\Delta_{1/2}$ of a spectral line is given by the following relation [32]:

$$\Delta\lambda_{1/2} = 2\omega\left(\frac{N_e}{10^{16}}\right) + 3.5A\left(\frac{N_e}{10^{16}}\right)^{1/4}$$

$$\times \left[1 - \frac{3}{4}N_D^{-1/3}\right]\omega\left(\frac{N_e}{10^{16}}\right), \qquad (2)$$

where ω is the electron impact width parameter, A is the ion broadening parameter, N_D is the number of particles in the Debye sphere and N_e is the electron number density. The first term on the right-hand side comes from the electron interaction, while the second term is generated by the ion interaction. Since the contribution of the ionic broadening is very small compared to the Stark broadening, it can be neglected. So the relation between electron number density and $\Delta_{1/2}$ of the Stark broadened line can be expressed by:

$$\Delta\lambda_{1/2} = 2\omega\left(\frac{N_e}{10^{16}}\right). \qquad (3)$$

The electron number densities (N_e) were calculated by the measurement of the FWHM of the Stark broadened Lorentz line shape of the ionic lines (393.37 nm) of Ca(II) in the four kinds of tea leaf samples. The value of ω corresponding to different electron temperatures can be obtained from the reference data [33]. The values of the electron temperatures and electron number densities in the four tea leaf samples are presented in Fig. 7.

As shown in Fig. 7, the electron temperatures and the electron number densities vary among the four tea samples. The Huangya sample exhibits the highest values for electron temperature with an averaged standard deviation value of 11735.9 ± 300.9 K. The electron temperatures for Longjing and Pu'er are 11456.1 ± 199.7 K and 11141.8 ± 324.9 K, respectively. The black tea sample sample exhibits a significantly lower value of electron temperature, 10892.1 ± 255.6 K. It is found that

Table 2. Spectroscopic parameters of the Ca(II) lines

Sr. No.	Wavelength λ (nm)	Transitions	Statistical weight g_k	Transition probability A_{ki} (s^{-1})	Energy (eV)	
					E_k	E_i
1	317.93	$3p^6 4d^2D_{3/2} \rightarrow 3p^6 4p^2P^0_{1/2}$	6	3.6×10^8	7.049150	3.150984
2	370.60	$3p^6 5s^2S_{1/2} \rightarrow 3p^6 4p^2P^0_{1/2}$	2	8.8×10^8	6.467875	3.123349
3	373.69	$3p^6 5s^2S_{1/2} \rightarrow 3p^6 4p^2P^0_{3/2}$	2	1.7×10^8	6.467875	3.150984
4	393.37	$3p^6 4p^2P^0_{3/2} \rightarrow 3p^6 4s^2S_{1/2}$	4	1.47×10^8	3.150984	0
5	396.85	$3p^6 4p^2P^0_{1/2} \rightarrow 3p^6 4s^2S_{1/2}$	2	1.4×10^8	3.123349	0
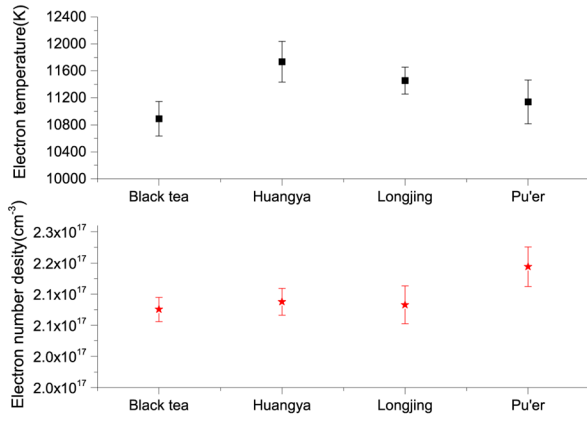
Fig.7 Electron temperatures and electron number densities in the four tea leaf samples at a 2 μs ICCD detection delay, 10 μs gate width and 50 mJ laser pulse energy. The error bars at each point represent the standard deviation

the sequence of electron temperatures of the four tea samples from high to low is exactly the same as the high to low sequence of their relative concentrations of the H element. A higher moisture content in the sample leads to a lower electron temperature. So it can be inferred that the sequence of moisture content in the four tea samples from high to low is black tea, Pu'er, Longjing and Huangya.

For the electron number density, the Pu'er sample has the highest electron number density of $(2.194\pm0.0318)\times10^{17}$ cm^{-3}. The Huangya and Longjing samples have similar electron number densities of $(2.138\pm0.0216)\times10^{17}$ cm^{-3} and $(2.133\pm0.0304)\times10^{17}$ cm^{-3} respectively, while the black tea leaf sample has the lowest of $(2.125\pm0.0195)\times10^{17}$ cm^{-3}. It can be deduced that the electron number density of the plasma may be directly correlated to the relative concentrations of mineral elements, for example K.

4.2 Local thermodynamic equilibrium

The use of emission spectroscopy for the determination of electron temperature and electron number density requires optically thin spectral lines. In this work, there is no dip at the central frequency of the observed emission lines. So it is assumed in our experiment that the plasma can be described by local thermodynamic equilibrium (LTE). The necessary condition for LTE that gives the corresponding lower limit of the electron number density N_e is given by the Mcwhirter criterion [34]:

$$N_e \geq 1.6 \times 10^{12} T^{1/2} (\Delta E)^3, \qquad (4)$$

where ΔE is the highest energy transition for which the condition holds and $T_e(\text{K})$ is the electron temperature. In our experiments, the electron temperature ranges from 10892 K to 11736 K and $\Delta E = 3.8986$ eV. The lower limit of the electron number density given by Eq. (4) is 1.0977×10^{16} cm^{-3}, while the electron number density in our work is on the order of 10^{17} cm^{-3}. Therefore, the assumption of LTE is validated.

5   Conclusion

In this paper, a 1064 nm wavelength Nd:YAG laser was used as the excitation source to ignite plasmas on black tea leaf, Huangya, Longjing and Pu'er samples, and a high resolution Czerny–Turner spectrometer and an ICCD detector were used for spectral separation and detection. Atomic, ionic and molecular spectra were found in these samples. The experimental results show that the intensities of the spectral lines increase monotonically with laser energy when the energy is lower than 50 mJ, but they clearly decrease when the laser energy exceeds 60 mJ because of the instabilities of the tablet pressed samples. The intensities of the ionic spectral lines decrease much faster than the atomic lines or molecular line with the delay time of the ICCD. The molecular spectrum of CN decreases the most slowly. It is also demonstrated that the RSDs of the relative concentrations in the tea samples are affected by the original shapes and structures of the tea leaf samples. Moreover, Pu'er has the highest relative concentrations of Mg, Mn, Al and K, and Longjing has the highest relative concentrations of Ca and Na, while black tea has the highest relative concentration of H. There are many possible reasons for the obvious differences in relative concentrations among the four samples, such as different degrees of fermentation, the local water and soil, as well as different moisture contents or some other parameters. In addition, the plasma parameters (electron temperature and electron number density) were determined to be around 11000 K and 10^{17} cm^{-3}, respectively. The results show that the LIBS technique is a new potential method for analyzing the compositions of tea leaf samples.

References

1   Li Xiuping, Li Lihua, Zhang Jinsheng, et al. 2005, Modern Instruments, 11: 27

2   Li Shubin. 2007, Chinese Journal of Spectroscopy Laboratory, 23: 1194

3   Fan Wenxiu, Li Xinzheng. 2006, Spectroscopy and Spectral Analysis, 25: 1714

4   Zheng Peichao, Liu Hongdi, Wang Jinmei, et al. 2014, Analytical Methods, 6: 2163

5   Zhang Lei, Hu Zhiyu, Yin Wangbao, et al. 2012, Frontiers of Physics, 7: 690

6   Wang Zhe, Yuan Tingbi, Hou Zongyu, et al. 2014, Frontiers of Physics, 9: 419

7   Lin Yongzeng, Yao Mingyin, Liu, Muhua, et al. 2012, Spectroscopy and Spectral Analysis, 32: 2925

8   Xu Yuan, Liu Muhua, Yao Mingyin, et al. 2012, Spectroscopy and Spectral Analysis, 32: 2555

9   Yao Mingyin, Huang Lin, Zheng Jianhong, et al. 2013, Optics & Laser Technology, 52: 70

10   Wu Jianglai, Lu Yuan, Li Ying, et al. 2011, Optoelectronics Letters, 7: 65

11   Li Ying, Wang Zhennan, Wu Jianglai, et al. 2012, Spectroscopy and Spectral Analysis, 32: 582

12 Yao Mingyin, Lin Jinlong, Liu Muhua, et al. 2012, Applied Optics, 51: 1552

13 Huang Lin, Yao Mingyin, Xu Yuan, et al. 2013, Applied Physics B, 111: 45

14 Zhu Dehua, Chen Jianping, Lu Jian, et al. 2012, Anal. Methods, 4: 819

15 Cai Yue, Chu Po-Chun, Ho Sutkam, et al. 2012, Frontiers of Physics, 7: 670

16 Wang Yang, Liu Weilong, Song Yunfei, et al. 2015, Chemical Physics, 447: 30

17 Jobiliong E, Suyanto H, Marpaung A M, et al. 2015, Applied Spectroscopy, 69: 115

18 Zhang Yiyang, Xiong Gang, Li Shuiqing, et al. 2013, Combustion and Flame, 160: 725

19 Yuan Ye, Li Shuiqing, Yao Qiang. 2015, Proceedings of the Combustion Institute, 35: 2339

20 Zhang Yiyang, Li Shuiqing, Ren Yihua, et al. 2015, Proceedings of the Combustion Institute, 35: 3681

21 Wang Qianqian, Liu Kai, Zhao Hua, et al. 2012, Frontiers of Physics, 7: 701

22 Zhang Dacheng, Ma Xinwen, Zhu Xiaolong, et al. 2008, Acta Physica Sinica, 57: 6348

23 Munson C A. 2005, Spectrochimica Acta Part B: Atomic Spectroscopy, 60: 1217

24 Morel S, Leone N, Adam P, et al. 2003, Applied Optics, 42: 6184

25 Baudelet M, Yu J, Bossu M, et al. 2006, Applied Physics Letters, 89: 163903

26 Aragon C, Aguilera J A, Penalba F, et al. 1999, Applied Spectroscopy, 53: 1259

27 NIST Atomic Spectra Database, http://www.physics. nist.gov/PhysRefData/ASD/lines-form.html

28 Samuels A C, DeLucia Jr F C, McNesby K L, et al. 2003, Applied Optics, 42: 6205

29 Baudelet M, Guyon L, Yu J, et al. 2006, Applied Physics Letters, 88: 063901

30 Bossu M, Hao Zuoqiang, Baudelet M, et al. 2007, Chinese Physics Letters, 24: 3466

31 Mohamed Walid T Y. 2008, Optics & Laser Technology, 40: 30

32 Hanif M, Salik M, Baig M A, et al. 2013, Optics and Spectroscopy, 114: 7

33 Griem H R. 1964, Plasma Spectroscopy. McGraw-Hill, New York, USA

34 McWhirter R W P. 1965, Plasma Diagnostic Techniques. Academic Press, New York, USA